Fully spin-polarized two-dimensional electron gas at the CoFe2 O4/ MgAl2 O4 (001) polar interface

Rémi Arras, Lionel Calmels

Fully spin-polarized two-dimensional electron gas at the $CoFe_2O_4/MgAl_2O_4(001)$ polar interface

R. Arras* and L. Calmels

CEMES, CNRS, and Université de Toulouse, BP 94347, F-31055 Toulouse, France

(Received 14 March 2014; revised manuscript received 27 May 2014; published 17 July 2014)

We performed first-principles calculations to show that a fully spin-polarized two-dimensional electron gas can be created at the interface between the polar and insulating spinel oxides $CoFe_2O_4$ and $MgAl_2O_4$. We give a clear description of the physical parameters (in particular the atomic termination of the interfaces), which favor the formation of this electron gas that is due either to an electric field induced in stoichiometric oxide layers because of their polar character or to a charge reorganization that preserves the global electric neutrality in nonstoichiometric layers. We show that the electric field-induced spin-polarized two-dimensional electron gas can only exist if the thickness of the $CoFe_2O_4$ layer is large enough and that it may be destroyed by intermixing at the interfaces.

DOI: 10.1103/PhysRevB.90.045411 PACS number(s): 73.20.−r, 71.30.+h, 75.50.Gg, 77.55.−g

I. INTRODUCTION

Interfaces between complex oxides can exhibit peculiar phenomena which may allow for the development of new fundamental physics and new electronic applications [1,2]. They can, for instance, promote the appearance of a two-dimensional electron gas (2DEG) [3,4], of superconductivity [5], or of magnetoelectric coupling in extrinsic multiferroic heterostructures [6]. Much effort has, in particular, been addressed to explain the thickness-dependent transition [7] which results in the appearance of a 2DEG at the now-famous interface between the nonmagnetic band insulators $LaAlO_3$ and $SrTiO_3$. Three scenarios have mainly been suggested for the existence of this 2DEG: the first one, in particular supported by first-principles calculations, is the presence of an electric potential which diverges as a function of the $LaAlO_3$ layer thickness, and which leads to an insulator-to-metal transition (IMT) above a critical thickness; two other scenarios concern the presence of oxygen vacancies or of interfacial atom intermixing which may induce a local charge doping (see, for example, Refs. [8] and [9] and references therein). It is also worth noting that magnetism has been experimentally evidenced in such a system [10], leading therefore to new perspectives for applications [1,2]. Subsequently, new heterostructures have been theoretically proposed to create highly spin-polarized 2DEG, replacing, for example, $SrTiO_3$ by FeS_2 [11] or EuO [12], or embedding a single monolayer of $LaMnO_3$ in $SrMnO_3$ [13]. Most of these compounds are unfortunately nonmagnetic or weakly magnetic, or possess a low Curie or Neel temperature: Highly spin-polarized 2DEG based on magnetic oxides keeping robust magnetic properties above room temperature are still missing.

In this paper, we propose investigating, with first-principles calculations, a couple of polar materials formed by the spinel oxides $CoFe_2O_4$ and $MgAl_2O_4$ to create fully spin-polarized 2DEG which may exist at high temperature. We will describe the electronic properties of different types of $CoFe_2O_4/MgAl_2O_4(001)$ supercells which differ by the structure of their interfaces. We will give a clear description of the physical parameters that favor the appearance of this 2DEG, which can be due either to the electric field generated in the stoichiometric oxide layers because of their polar character and charge discontinuities at the interfaces, or due to a charge reorganization at the interfaces which preserves the electric neutrality when the layers are symmetric but not stoichiometric. We finally show that the internal electric field can be lowered by interface intermixing.

$MgAl_2O_4$ is a well known insulating and nonmagnetic substrate with a normal spinel structure of formula $[Mg^{2+}]_A[Al_2^{3+}]_BO_4^{2-}$. The subscripts A and B denote, respectively, the tetrahedral and octahedral atomic sites, which are defined by the face-centred-cubic lattice of oxygen atoms. The conventional cubic cell of $MgAl_2O_4$ contains eight formula units and presents a succession of alternating $[Mg_A]^{2+}$ and $[(Al_2)_BO_4]^{2-}$ atomic layers in the (001) direction.

$CoFe_2O_4$ is a particularly attractive insulator, with good magnetostrictive properties [14,15] and a ferrimagnetic order that is preserved up to the high Curie temperature $T_C = 793$ K. The cation distribution inside the oxygen lattice of $CoFe_2O_4$ is close to the inverse spinel structure of formula $[Fe^{3+}]_A[Co^{2+},Fe^{3+}]_BO_4^{2-}$ and in the (001) direction, its cubic cell is composed of an alternation of four $[Fe_A]^{3+}$ and $[(FeCo)_BO_4]^{3-}$ atomic bilayers. $CoFe_2O_4$ has already been grown on different oxide substrates ($MgAl_2O_4$, $SrTiO_3$, $LaAlO_3$, α-Al_2O_3, MgO) [16–21]. $MgAl_2O_4(001)$ is a particularly suited substrate for such a growth because of its similar structure and lattice parameter (only 3.8% lower than that of $CoFe_2O_4$): Pseudomorphic growth of $CoFe_2O_4$ has already been reported on $MgAl_2O_4(001)$, with a good crystalline structure and for thicknesses as small as a few nanometers [22]. $MgAl_2O_4(001)$ thin films have also been grown on spinel oxides and associated with $CoFe_2O_4$ in spin-filtering heterostructures [23].

Different studies based on the density functional theory (DFT) have already been performed to understand the properties of bulk cubic $CoFe_2O_4$, of its tetragonally distorted strained cristal [24–26], and of multilayers associating $CoFe_2O_4$ with half-metallic Fe_3O_4 [27] or with Au metallic layers [28]. DFT methods are, however, difficult to use for this oxide: The strongly correlated character of the $3d$ electrons requires the use of complex methods like the DFT + U [25,26,29–31], and the random distribution of Co and Fe atoms in octahedral atomic sites is complicated to take into account.

*remi.arras@cemes.fr

II. DETAILS OF THE CALCULATIONS

Our calculations were performed with the full-potential linearized augmented plane-waves code WIEN2K [32]. We have systematically used the generalized gradient approximation (GGA) [33], with the fully localized and rotationally invariant "$+U$" correction [34,35] applied on $3d$ electrons. The parameter $U_{\text{eff}} = U - J$ was set to 3.94 eV for all Fe and Co atoms. The atomic sphere radii have been set to 1.8 atomic units (a.u.) for Fe and Co, 1.6 a.u. for Al and Mg, and to 1.4 a.u. for O atoms. We used the parameter $R_{\text{min}}K_{\text{max}} = 7$, the product of the smallest atomic sphere radius R_{min} by the plane-wave cutoff K_{max} for the plane-wave expansion in the interstitial area.

When no more details are given, we used the distribution of cations which corresponds to the $Imma$ space group in bulk $CoFe_2O_4$ [25], and we applied the (001) tetragonal distortion in such a way that the structure is reduced to the $C2/c$ space group, in superlattices with a total length of approximately 2.56 nm. In the case of stoichiometric and asymmetric $CoFe_2O_4/MgAl_2O_4$ supercells, we studied the modifications of the physical properties as a function of the layer thicknesses or for different cation distributions.

For each superlattice, the length in the [001] direction has been calculated by energy minimization, starting from the supercell length estimated from the bulk lattice parameters of tetragonal $CoFe_2O_4$ and cubic $MgAl_2O_4$. A complete relaxation of the atomic coordinates has also been done with a reduction of the applied forces down to 5 mRy/bohr.

The irreducible wedge of the first Brillouin zone was sampled with 72 k points for the bulk cubic cells, and around 20 k points parallel to the interfaces were used for the supercells.

In the following, we only consider $CoFe_2O_4$ layers strained on a $MgAl_2O_4(001)$ substrate with its calculated lattice parameter of 8.18 Å (8.08 Å in experiments). The calculated 3.8% lattice mismatch between these two materials is very close to the experimental value. This mismatch induces a tetragonal distortion which increases the $CoFe_2O_4$ lattice parameter in the [001] direction (z axis) up to the value of 8.83 Å. This corresponds to a tetragonal distortion of 7.9%, which can be compared to the value of $6.2\% \pm 0.3\%$ measured by Matzen *et al.* [19] This distortion does not strongly modify the density of states (DOS) of $CoFe_2O_4$ and its spin magnetic moments only change by less than 1% (see Appendix A).

We will consider the influence of $CoFe_2O_4/MgAl_2O_4(001)$ interfaces with different atomic terminations. Each supercell is electrically neutral and contains two interfaces which can be nonequivalent, and only the association of these interfaces is relevant for the small oxide layer thicknesses we considered. The usual succession of atomic layers for a spinel structure is preserved across the interfaces.

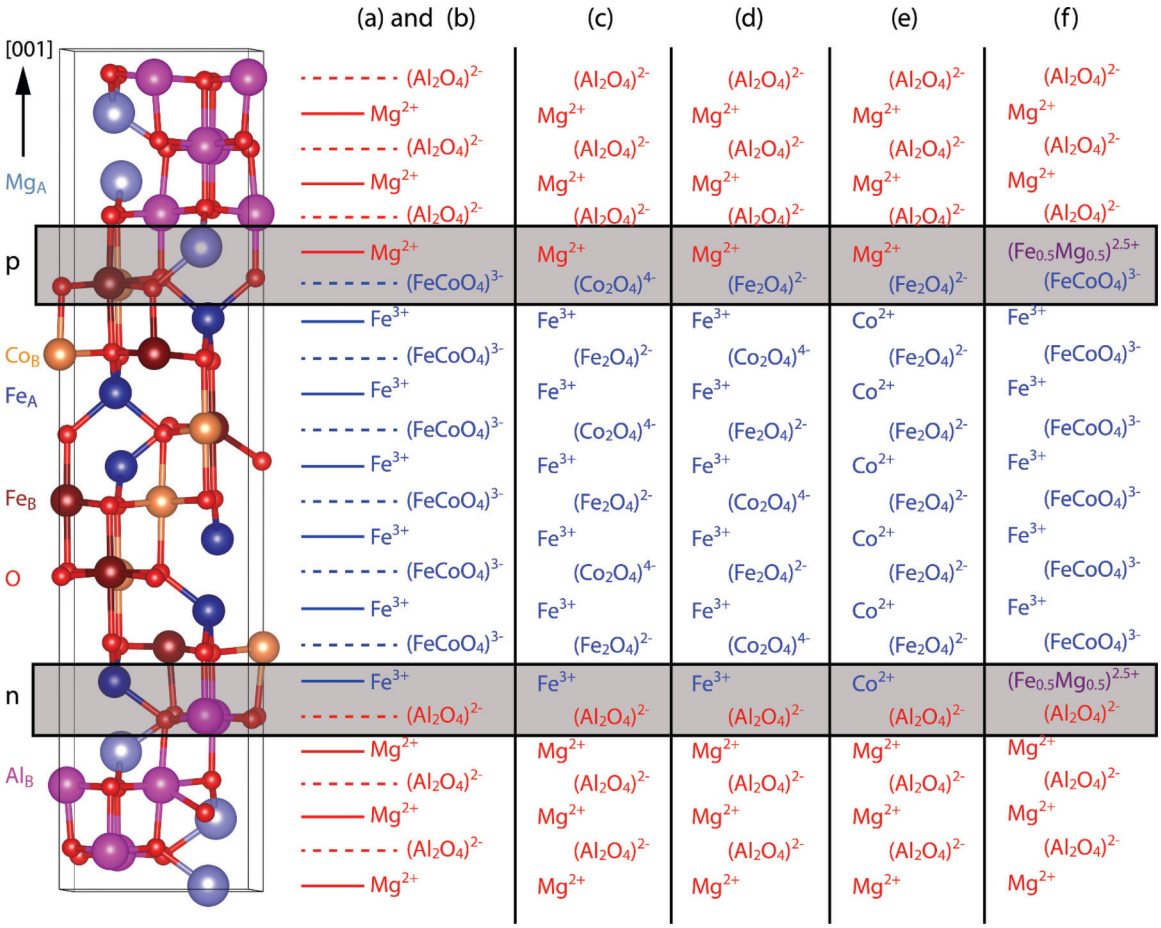

FIG. 1. (Color online) On the left, the $CoFe_2O_4/MgAl_2O_4(001)$ 6/6 supercell with six atomic bilayers of $CoFe_2O_4$ and six bilayers of $MgAl_2O_4$, separated by one p-type $[Mg_A/(FeCo)_BO_4]$ and one n-type $[Fe_A/(Al_2)_BO_4]$ interface and the alternation of atomic planes corresponding to Table I(a) and I(b). On the right, the same superlattice with different cation distributions in $CoFe_2O_4$ [Table I(c) to I(f)].

III. RESULTS

A. Asymmetric supercells and thickness-dependent insulator-to-metal transition

The first superlattice, which contains six atomic bilayers of $CoFe_2O_4$ and six bilayers of $MgAl_2O_4$ (6/6) in the [001] stacking direction, is shown on the left-hand side of Fig. 1. The two interface terminations are $[Mg_A]^{2+}/[(FeCo)_BO_4]^{3-}$ (p interface) and $[Fe_A]^{3+}/[(Al_2)_BO_4]^{2-}$ (n interface). This superlattice is asymmetric and contains stoichiometric oxide layers. Because of this asymmetry and of the charge discontinuity at the two interfaces, chemical charges with a density $\pm\sigma_c$ exist at the two interfaces, giving rise to an electric field E with opposite directions in $CoFe_2O_4$ and $MgAl_2O_4$, as it can be seen on the DOS curves shown in Fig. 2. The value of this electric field has been estimated to 106 mV/Å from the slope of the z dependent locally averaged electrostatic potential shown in Fig. 3. It is very close to the theoretical value $E = \sigma_c/\varepsilon_0(\varepsilon_r^{MAO} + \varepsilon_r^{CFO})$ of 110 mV/Å, where $\sigma_c =$ 0.5 electron per two-dimensional unit cell (according to the ionic model of $CoFe_2O_4$ and $MgAl_2O_4$), ε_0 is the vacuum permittivity and $\varepsilon_r^{MAO} = 7.89$ and $\varepsilon_r^{CFO} = 16.64$ are the relative permittivities of $MgAl_2O_4$ [36] and $CoFe_2O_4$ [37]. The calculated relaxation shows that the averaged z coordinate is slightly different for the cation and anion nuclei within a given atomic layer. The displacement of the cation and anion nuclei is due to interface effects and to the internal electric field resulting from the polar character of the oxide interfaces. The displacement of the nuclei is on average higher for oxygen than for metallic atoms. In any case, it does not exceed 0.07 Å.

By increasing the thickness of the $CoFe_2O_4$ and $MgAl_2O_4$ layers, we can expect that the buildup potential leads to a "polar catastrophe" phenomenon similar to that found in the $LaAlO_3/SrTiO_3$(001) superlattices [38]. According to the schematic view displayed in Fig. 4, an IMT should occur above a critical $CoFe_2O_4$ thickness, with a transfer of electrons from the Co^{2+} atoms at the p interface to the Fe_B^{3+} atoms at the n interface, with $MgAl_2O_4$ remaining insulating. This charge transfer should only involve the minority spin channel because of its lowest band gap. Considering the ionic model of $CoFe_2O_4$, 0.5 electron per two-dimensional unit cell must be transferred to counterbalance the chemical charge σ_c and to suppress the electric field. We found that the transfer should occur for a $CoFe_2O_4$ layer thickness above approximately 19 Å [i.e., 9 $Fe_A/(Fe,Co)_BO_4$ bilayers].

To check these assumptions, we increased the supercell thickness from 6/6 to 8/8 and 10/10 bilayers (see the band structures in Fig. 5) and found that the IMT has already occurred for the largest of these three supercells, which contains 10 $Fe/FeCoO_4$ bilayers. In this superlattice, the electric field has decreased to 0.71 mV/Å, which corresponds to a charge transfer of 0.165 electron per two-dimensional unit cell (this charge would increase up to 0.5 electron for thicker $CoFe_2O_4$ layers). The quasi-2DEG which is created at the n interface extends over three $FeCoO_4$ atomic layers, with a spin-polarization of -100%. The corresponding state

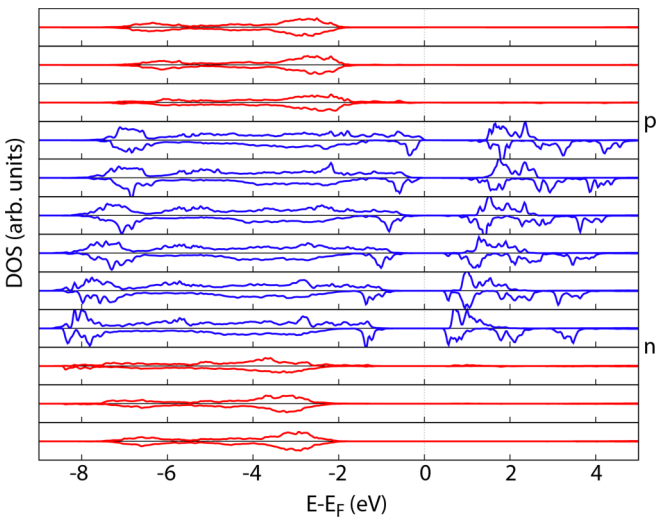

FIG. 2. (Color online) Total density of states projected on the successive atomic bilayers of the 6/6 supercell. The blue curves correspond to the $CoFe_2O_4$ layer, and the red curves to the $MgAl_2O_4$ layer, while the positive and negative curves correspond, respectively, to majority and minority spin electrons.

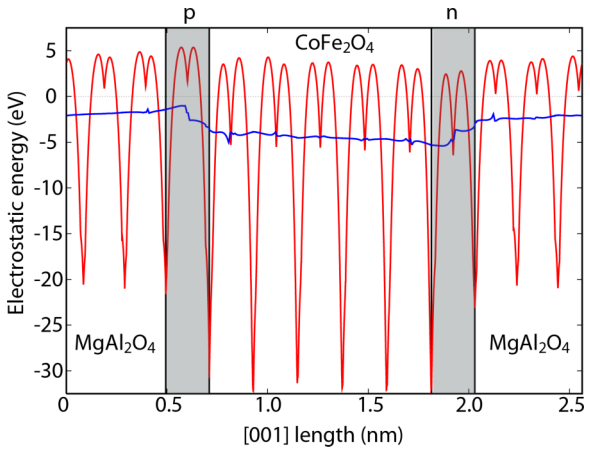

FIG. 3. (Color online) (x,y)-averaged electrostatic Coulomb potential as a function of the z coordinate, perpendicular to the interfaces (red curve) and its local z-averaged value (blue curve) for the 6/6 supercell.

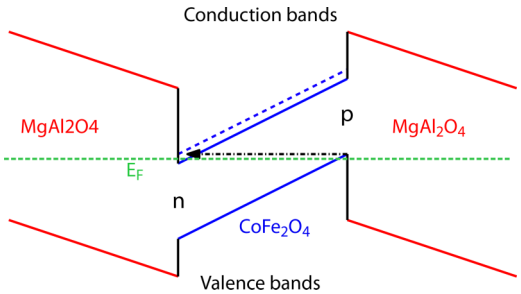

FIG. 4. (Color online) Diagram of the IMT which corresponds to a transfer of electrons from the top of the valence band at the p interface to the bottom of the conduction band at the n interface. This transfer involves the minority spin channel electrons of $CoFe_2O_4$ (blue solid line), and not the majority spin (blue dashed line).

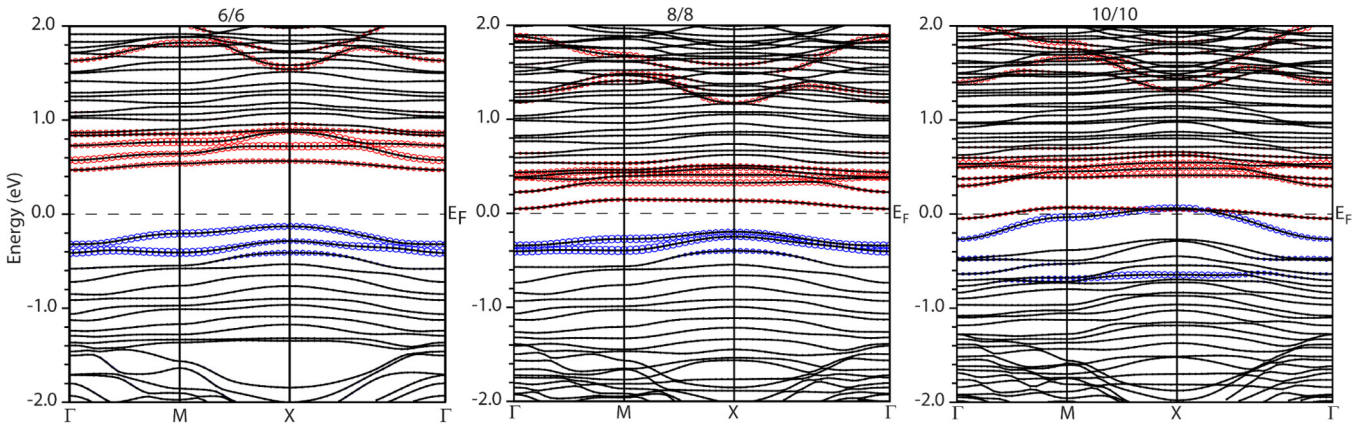

FIG. 5. (Color online) Minority spin band structures for the 6/6, 8/8, and 10/10 stoichiometric and asymmetric $CoFe_2O_4/MgAl_2O_4(001)$ supercells. The contributions of the Fe_B atoms at the n interface, and of the Co_B atoms at the p interface are, respectively, represented by red and blue circles.

at the Fermi energy (E_F) mainly involves d_{xz} orbitals of Fe_B atoms. For another cation distribution, corresponding to the bulk space group $P4_122$, the Fe_B-d_{xz} and d_{yz} bands would be degenerated and equally occupied (see Appendix B). At the same time, the minority spin Co-d_{xy} bands at the p interface are pushed upwards in energy and cross E_F, creating a two-dimensional hole gas strongly localized on the p-interface $FeCoO_4$ atomic layer and also with a -100% spin polarization. Figure 5 shows that the band crossing E_F at the p interface has a wider dispersion (a smaller averaged effective mass $m_h^* = 3.21\ m_0$ at X, m_0 being the free electron mass) than the band at the n interface ($m_e^* = 4.64\ m_0$ at Γ).

B. Influence of the cation distribution in $CoFe_2O_4$

We studied the influence of the distribution of Co and Fe ions in the $CoFe_2O_4$ layer on the different properties of the 6/6 supercell (see Table I with the corresponding stackings in Fig. 1). The cation distributions displayed in Table I(a) and I(b) both correspond to a $CoFe_2O_4$ layer with inverse spinel structure and similar $Mg/(FeCoO_4)$ p-type and $Fe/(Al_2O_4)$ n-type interfaces; they therefore show similar behavior (see Appendix A) and equivalent electric fields. The critical thickness for the IMT may, however, change drastically with a change in the chemical composition of each atomic layer parallel to the interfaces.

TABLE I. Total energy differences per $CoFe_2O_4$ formula unit, between the 6/6 supercells with different cation distributions in $CoFe_2O_4$ (the total energy for the space group $C2/c$ is taken as a reference), electric field in the [001] direction, and total spin-resolved band gap around the Fermi level. The atomic structures corresponding to the different lines of the table are shown in Fig. 1.

	Bulk tetragonal $CoFe_2O_4$ space group	ΔE in meV	Electric field in mV.Å^{-1}	band gap majo. in eV	band gap mino. in eV
(a)	$C2/c$	0	106	0.64	0.59
(b)	$P4_122$	−70	107.5	0.79	0.53
(c)	$Imma$	+94	93	0.74	0.00
(d)	$Imma$	−33	<5	1.64	0.86
(e)	$I41/amd$	+33	0	2.67	1.29
(f)	$C2/c$	−103	0	1.64	1.11

In the stoichiometric $CoFe_2O_4$ layer with inverse spinel structure, the electric field can be modified with a different cation distribution inside the octahedral atomic sites. For the 6/6 supercells and the $Imma$ tetragonal space group, the IMT has already occurred in the case of a Co-rich p interface [see Table I(c)]: The 2DEG created in this case at the n interface is located on a single atomic layer with a strong Fe_B-d_{xy} character and a band dispersion ($m_e* = 0.62$ m$_0$) wider than that of the two-dimensional hole gas ($m_h* = 2.3$ m$_0$). The critical thickness is smaller in this case than when the p interface contains the same number of Fe and Co atoms [Table I(a) and I(b)]. Conversely, the internal electric field is almost suppressed with a Fe-rich p interface [Table I(d)].

The distribution of cations between tetrahedral and octahedral sites is also important. The internal electric field is caused by the fact that we chose on one side of the interface a normal spinel and on the other side an inverse spinel, which imposes a charge discontinuity across the interfaces. Reducing the degree of inversion of $CoFe_2O_4$ reduces the electric field which vanishes when $CoFe_2O_4$ is a perfect normal spinel [Table I(e)].

C. Influence of interface intermixing

We considered a stoichiometric supercell with an intermixing between cations from $MgAl_2O_4$ and from $CoFe_2O_4$; the two identical interfaces contain a combination of Mg_A and Fe_A atoms [Table I(f)] and an electric charge of 2.5 electrons, intermediate between those of pure Fe_A and Mg_A layers. The electric field is, in this case, suppressed. The DOS (not shown) does not display any gap states, and the calculated magnetic moments stay approximately the same as in bulk $CoFe_2O_4$.

D. Off-stoichiometric layers

To finish, we considered symmetric supercells with two identical p or two identical n interfaces. By construction, these superlattices do not preserve the stoichiometry of

the two materials. As a consequence, some atoms of the $CoFe_2O_4$ layer experience a local charge doping (the supercell staying electrically neutral) and an half-metallic interface state appears. The nonstoichiometry can be seen as resulting from an atomic layer substitution: In the case of a superlattice with two p interfaces, an entire atomic layer of Fe_A atoms has been substituted by a Mg_A layer, and conversely with a superlattice with two n interfaces. For the p (n) interfaces, we thus observe a variation of the total magnetic moment of $+6\ \mu_B$ ($-6\ \mu_B$) per substituted Fe^{3+} (Mg^{2+}) ion, $+5\ \mu_B$ ($-5\ \mu_B$) being due to the substituted cation, and $+1\ \mu_B$ ($-1\ \mu_B$) to the reorganization of charges that keep the total system electrically neutral. This simple two-step mechanism, which is here described in the approximation of the perfect ionic model, suits well with previous results obtained by DFT calculations on noncharged structural defects in magnetite Fe_3O_4 [39]. Here, the reorganization of charges, in this approximation, corresponds for the p (n) interface to the transition $Co^{2+} \rightarrow Co^{3+}$ ($Fe^{3+} \rightarrow Fe^{2+}$). The rebalanced charge is equally split between the two equivalent interfaces; it is responsible for the appearance of -100%-spin polarized gap states which can be seen in the DOS curves of Fig. 6. It is accompanied by an increase of the magnetic moment of Co atoms at the p interface of approximately 12% and by a decrease of the magnetic moments of all the Fe_B of the n supercell of 2.5% on average. The gap states which cross the Fermi level have the same contribution as for the asymmetric superlattice: Fe_B $d_{xz}(+d_{yz})$ or Co_B d_{xy} orbitals.

IV. DISCUSSION

We have described heterostructures with different atomic distributions and interface terminations. We have shown that a strong electric field is created in asymmetric and stoichiometric supercells with sharp interfaces. A buildup potential which diverges as a function of the layer thickness appears in this case. As it has been suggested for the well-studied $LaAlO_3/SrTiO_3(001)$ system, different scenarios can be proposed to change the electrical boundary conditions at the interfaces and avoid the polar catastrophe.

The first mechanism that we considered consists of an electron transfer from the Co p-type to the Fe n-type interface atoms. This mechanism is made possible due to the two different degrees of oxidation ($+2$ and $+3$) accessible for these cations. The second mechanism which avoids the polar catastrophe involves atomic reconstructions. Three different kinds of atomic reconstructions have been considered: Atomic site exchanges [$CoFe_2O_4$ changing from inverse to normal spinel structure, Table I(e)], which cancels the charge discontinuities, intermixing resulting in two equivalent interfaces and a suppression of the stoichiometric $CoFe_2O_4$ layer asymmetry [Table I(f)], and finally off-stoichiometric supercells in which the asymmetry has also disappeared, but where substitutions locally dope the $CoFe_2O_4$ atomic layer at the interface (see Sec. III D). If the electronic reconstruction scenario coincides with a thickness-dependent IMT, this is not the case of the situations where atomic reconstructions occur. Atomic reconstructions can, however, encourage the appearance of a two-dimensional electron or hole gas.

Only considering stoichiometric and asymmetric supercells, the cation distribution which has the lowest energy corresponds to the space group $P4_122$ for bulk $CoFe_2O_4$. The comparison between supercells with similar bulk cation distributions, but different interface terminations [Table I(a) and I(f) or I(c) and I(d)], shows that the stackings which have the lowest energy are those in which the internal electric field is lowered or suppressed by a suitable choice of interface atomic structure. The symmetric configuration with atomic intermixing has the lowest energy over all the stoichiometric supercells (the different number of atoms does not allow a direct comparison with the off-stoichiometric supercells).

All the interfaces described in Table I deserve, however, to be studied because they may exist in real samples, even if their energy is slightly higher: growth techniques being usually based on out-of-equilibrium processes, they may allow the stabilization of all these interfaces, including those with internal electric fields. The atomic structure of real samples is probably

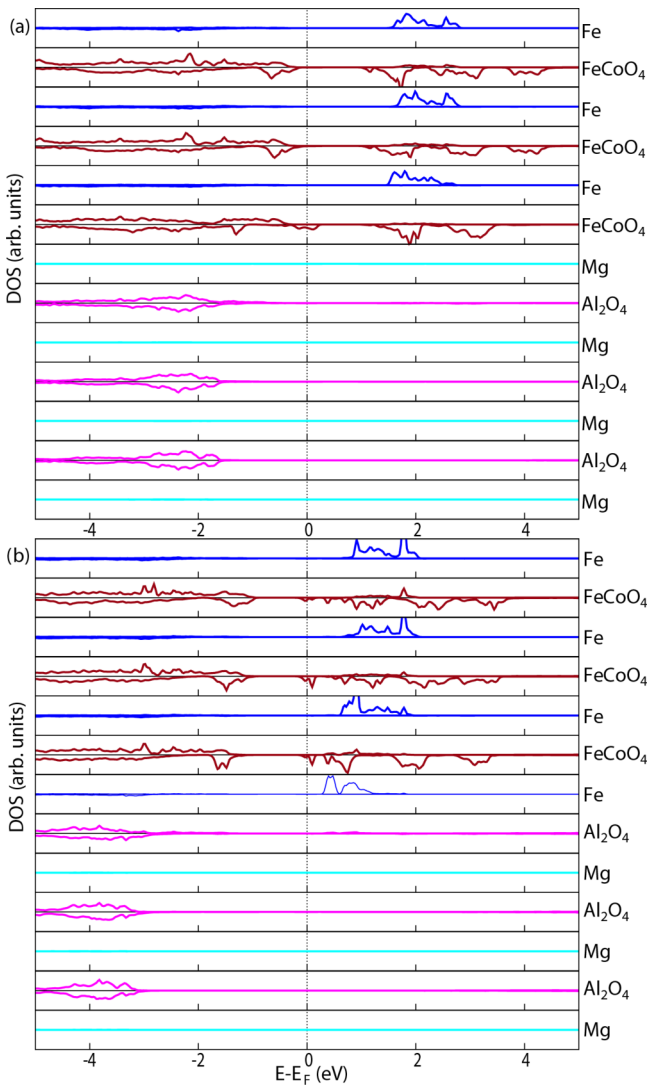

FIG. 6. (Color online) Layer-resolved densities of states for half of the nonstoichiometric supercells with (a) two p interfaces and (b) two n interfaces.

intermediate between the ideal configurations described above. The detailed atomic structure and the value of the electric field will depend on the mechanisms (compensation of the interface electric dipoles after the growth or energetic mechanisms during the growth) which have induced these reconstructions. Until now, different experimental studies have shown that the degree of inversion of $CoFe_2O_4$ is in general in the range of 80–90%, depending mostly on the growth conditions: Using x-ray magnetic circular dichroism experiments, Matzen *et al.* [19] found, for example, an inversion degree of 90% for 5-nm-thick layers grown on $MgAl_2O_4(001)$. A partial cation intermixing should also certainly occur at the $CoFe_2O_4/MgAl_2O_4$ interfaces, but the probability that it fulfills simultaneously all the conditions required to cancel completely the internal electric field (perfect interface mixing with a preservation of the symmetry of the $CoFe_2O_4$ layer) is low. Some works on the $LaAlO_3/SrTiO_3$ system have also suggested that cation intermixing at the interfaces could be thermodynamically stable [40–42]. However, such intermixing is not necessarily contraindicated to stabilize a 2DEG, as it may locally change the stoichiometry and induce charge reorganizations and lattice distortions. The diffusion of Al or Mg atoms in $CoFe_2O_4$ could modify the oxidation degree of Co and Fe cations to equilibrate electric charges, following similar processes as those described in Sec. III D. By changing the stoichiometry of $CoFe_2O_4$, our results indeed suggest that it is possible to vary locally its magnetization, and certainly its conductivity via hole or electron doping. This would be in good agreement with experimental measurements reported on iron-doped [43] or oxygen-deficient [44] $CoFe_2O_4$.

We made lots of comparisons between the $CoFe_2O_4/MgAl_2O_4$ heterostructure and the $LaAlO_3/SrTiO_3$ system, for which numerous studies already exist. The exact mechanisms that could explain the conductivity of the $LaAlO_3/SrTiO_3$ interface are still under debate [9]. Experimental measurements focusing on the conductivity of the $CoFe_2O_4/MgAl_2O_4(001)$ interface have not been reported up to now. By making an analogy with half-metallic magnetite Fe_3O_4 for the n interface, when the Fe_B atoms are doped with electrons (after the IMT has occured or for off-stoichiometric supercells), we can expect a double-exchange conduction mechanism to occur, in which electrons would jump between Fe_B^{2+} and Fe_B^{3+} ions [45,46]. This would be consistent with the interface half-metallic behavior that has been calculated. Increasing the content of Fe cations would obviously increase the conductivity by counterbalancing the cation disorder created by Co atoms. Crucial experimental data on the atomic structure of the $CoFe_2O_4/MgAl_2O_4$ interface which could be obtained by scanning transmission electron miscroscope (STEM) annular dark field (ADF) and electron energy loss microscopy (EELS) techniques [40] are missing and would help to understand how this system really behaves.

V. CONCLUSION

In conclusion, we have shown that minority spin two-dimensional electron and hole gas can be created at the interfaces between the insulating normal and inverse spinel oxides $MgAl_2O_4$ and $CoFe_2O_4$. In the case of asymmetric, but stoichiometric layers, an internal electric field appears due to the charge discontinuities at the interfaces, and it induces in $CoFe_2O_4$ an IMT, which is found to occur for a $CoFe_2O_4$ thickness larger than 19 Å (different values of U_{eff} would slightly change this critical thickness). A two-dimensional electron gas can also be stabilized by charge doping by varying the relative contents of Fe, Co, or O atoms near the interfaces. A good control of the growth of $CoFe_2O_4/MgAl_2O_4$ multilayers stays, however, very challenging. In particular, different cation distributions inside $CoFe_2O_4$, or some intermixings between atoms from this material and from $MgAl_2O_4$ are likely to lower the electric field by changing the symmetries or the charge on each atomic layers. We hope that this work will encourage fine experimental characterization of the spinel-spinel interfaces.

ACKNOWLEDGMENTS

The authors want to thank J.-B. Moussy for helpful discussions. The authors of this work were granted access to the HPC resources of CALMIP under the allocations P1313 and P1229 (2012-2014) and GENCI-CINES (Grant No. 2013-c2013096949).

APPENDIX A: CATION DISRIBUTIONS AND PROPERTIES OF BULK $CoFe_2O_4$

We considered two different cation distributions in the perfect inverse spinel $CoFe_2O_4$ cubic crystals, with the space groups $Imma$ (No. 74) and $P4_122$ (No. 91) (we used the space groups from the Bilbao crystallographic server [47]).

For the space group $P4_122$, the three $\langle 100 \rangle$ directions are equivalent and the lattice is composed by a succession of $[Fe_A]^{3+}/[(Co,Fe)_BO_4]^{3-}$ $\{100\}$ bilayers. The situation is different for the space group $Imma$: $CoFe_2O_4$ presents an alternation of $[Fe_A]^{3+}$ and $[(Co,Fe)_BO_4]^{3-}$ (100) or (001) atomic layers, and a different alternation of $[Fe_A]^{3+}$ and either $[(Co_2)_BO_4]^{4-}$ or $[(Fe_2)_BO_4]^{2-}$ (010) atomic layers.

The tetragonal distortion results from an in-plane compressive strain: The in-plane lattice parameter of $CoFe_2O_4$ is equal to the calculated cubic parameter of $MgAl_2O_4$, and the lattice parameter in the perpendicular direction is found by a minimization of the total energy. The space group does not change when the tetragonal axis is along any of the $\langle 100 \rangle$ equivalent directions of the $P4_122$, or along the [010] direction of the $Imma$ cubic cells. The situation is different when the tetragonal distorsion is along the [100] or the [001] directions of the $Imma$ cell: In this case, the symmetry is lowered and the space group becomes $C2/c$ (No. 15).

The bulk tetragonally distorded $CoFe_2O_4$ crystal thus consists of the following:

(1) An alternation of $[Fe_A]^{3+}$ and $[(Fe,Co)_BO_4]^{3-}$ atomic layers perpendicular to the tetragonal axis, with space group $C2/c$ or $P4_122$;

(2) Or a period of four atomic layers $[Fe_A]^{3+}/[(Fe_2)_BO_4]^{2-}/[Fe_A]^{3+}/[(Co_2)_BO_4]^{4-}$ perpendicular to the tetragonal axis, for the space group $Imma$.

The calculated physical properties of the cubic and tetragonally distorted bulk $CoFe_2O_4$ crystals are given in Table II for

TABLE II. Differences between the total energies per formula unit calculated for different cation distributions in $CoFe_2O_4$ (the total energy for the space group $P4_122$ is taken as a reference for the cubic and the tetragonal cells), lattice parameters in the [001] direction, band gap energies near the Fermi level and atomic spin magnetic moments. Some results for the normal spinel are also given for comparisons (denoted by a *).

Cell	Space group	ΔE (in meV/f.u.)	$a^{[001]}$ (in Å)	band gap at E_F (in eV) Majority spin	Minority spin	magnetic moments (in μ_B) Fe_A (Co_A*)	Fe_B	Co_B (Fe_B*)	O_1	O_2
Cubic	$Imma$	+10	8.493	1.97	1.02	−3.88	4.01	2.57	0.08	0.02
	$P4_122$	0	8.514	1.97	1.32	−3.89	4.01	2.58	0.07	0.03
	$Fd\bar{3}m$*	+83	8.556	2.67	1.38	−2.49*	4.05	4.05*	0.22	0.22
Tetragonal	$Imma$	−12	8.854	1.72	0.87	−3.87	3.99	2.56	0.09	0.02
	$C2/c$	−33	8.833	1.74	0.99	−3.86	3.99	2.56	0.08	0.03
$a^{[100]} = a^{[010]}$	$P4_122$	0	8.833	1.77	1.20	−3.87	3.99	2.57	0.07	0.03
= 8.18 Å	$I41/amd$*	158	8.979	2.62	1.14	−2.47*	4.04	4.04*	0.23	0.23

different cation distributions. The corresponding DOS curves can be seen in Fig. 7.

In agreement with previous results published by Fritsch and Ederer [26], we find that the cation distribution corresponding to the cubic cell with space group $P4_122$ is the most stable. Such cation ordering has already been evidenced by Raman spectroscopy in the $NiFe_2O_4$ compound [48,49]. Most recent Raman measurements confirmed the inverse character of $CoFe_2O_4$ and that a cation ordering would also exist at octahedral sites in this material [50].

Our calculated band-gap energies and magnetic moments are close to those calculated by other groups [25,51–53], and to the experimental indirect band gap of 1.2 eV measured by optical measurements [52]. The calculated band gap of $MgAl_2O_4$ is of 5.13 eV, lower than the 7.8 eV measured experimentally and reported in Ref. [54].

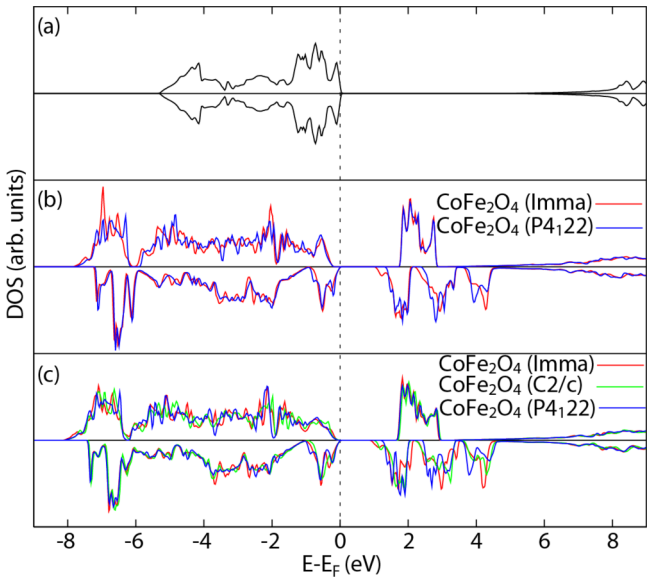

FIG. 7. (Color online) Density of states for majority spin (positive curves) and minority spin electron (negative curves) for (a) bulk $MgAl_2O_4$, (b) bulk cubic $CoFe_2O_4$, and (c) bulk tetragonal $CoFe_2O_4$.

APPENDIX B: ORBITAL DEGENERACIES AND OCCUPANCIES

Several differences can be observed between the electronic structures calculated for different cation distributions in the $CoFe_2O_4$ crystal, especially concerning the occupancy of the different d orbitals after the IMT.

The minority spin band gap is, for instance, 0.3 eV lower for the $Imma$ than for the $P4_122$ space group. This can be explained in terms of the splitting of the d-t_{2g} orbitals for the $Imma$ space group (see Fig. 7) due to the nonequivalent cation distribution along the three ⟨100⟩ directions.

We performed bulk calculations for $CoFe_2O_4$ crystals in which we added or subtracted one electron to check the consequences of interface charge doping. An additional electron will equally occupy the Fe_B-d_{xz} and d_{yz} orbitals in $CoFe_2O_4$ with $P4_122$ space group (the z axis corresponding to the tetragonal axis), only the Fe_B-d_{xz} orbitals for $C2/c$, and only the Fe_B-d_{xy} orbitals for $Imma$ (see Table III). In the two last cases, the above-mentioned orbitals lie in $(Fe_2)_BO_4$ atomic layers. They are oriented along equivalent directions with respect to the cation distribution, which thus controls the orbital occupancy. This will induce different degrees of charge localization near the interfaces.

These cation distribution have also been proposed and described by Fritsch and Ederer in Refs. [25] and [26].

The effects of a different cation distribution in $CoFe_2O_4$ can be more important in thin films with interfaces than in bulk crystals. The consequences of a modification of the cation distribution are, however, small when the electric charge on each atomic layer parallel to the interfaces is preserved: The

TABLE III. Occupied d orbitals when the number of electrons is modified in bulk tetragonally distorted $CoFe_2O_4$.

Space group	Occupied orbital $-1e$	$+1e$
$Imma$	Co $d_{xz} + d_{yz}$	Fe d_{xy}
$C2/c$	Co $d_{xy} + d_{yz}$	Fe d_{xz}
$P4_122$	Co d_{xy}	Fe $d_{xz} + d_{yz}$

physical behavior stays in this case more or less the same (as an example, the electric fields calculated in the $P4_122$ and $C2/c$ 6/6 supercells are nearly the same), but become stronger otherwise.

[1] J. Mannhart and D. G. Schlom, Science **327**, 1607 (2010).

[2] D. F. Bogorin, P. Irvin, C. Cen, and J. Levy, *$LaAlO_3/SrTiO_3$-Based Device Concepts* (Oxford University Press, New York, 2012), Chap. 13.

[3] A. Ohtomo, D. A. Muller, J. L. Grazul, and H. Y. Hwang, Nature (London) **419**, 378 (2002).

[4] A. Ohtomo and H. Y. Hwang, Nature (London) **427**, 423 (2004).

[5] N. Reyren, S. Thiel, A. D. Caviglia, L. F. Kourkoutis, G. Hammerl, C. Richter, C. W. Schneider, T. Kopp, A.-S. Retschi, D. Jaccard, M. Gabay, D. A. Muller, J.-M. Triscone, J. Mannhart, Science **317**, 1196 (2007).

[6] J. D. Burton and E. Y. Tsymbal, Phil. Trans. R. Soc. A **370**, 4840 (2012).

[7] S. Thiel, G. Hammerl, A. Schmehl, C. W. Schneider, and J. Mannhart, Science **313**, 1942 (2006).

[8] S. A. Pauli and P. R. Willmott, J. Phys.: Cond. Matter **20**, 264012 (2008).

[9] D. G. Schlom and J. Mannhart, Nat. Mater. **10**, 168 (2011).

[10] A. Brinkman, M. Huijben, M. van Zalk, J. Huijben, U. Zeitler, J. C. Maan, W. G. van der Wiel, G. Rijnders, D. H. A. Blank, and H. Hilgenkamp, Nat. Mater. **6**, 493 (2007).

[11] J. D. Burton and E. Y. Tsymbal, Phys. Rev. Lett. **107**, 166601 (2011).

[12] Y. Wang, M. K. Niranjan, J. D. Burton, J. M. An, K. D. Belashchenko, and E. Y. Tsymbal, Phys. Rev. B **79**, 212408 (2009).

[13] B. R. K. Nanda and S. Satpathy, Phys. Rev. Lett. **101**, 127201 (2008).

[14] R. M. Bozorth, E. F. Tilden, and A. J. Williams, Phys. Rev. **99**, 1788 (1955).

[15] Y. Chen, J. E. Snyder, C. R. Schwichtenberg, K. W. Dennis, R. W. McCallum, and D. C. Jiles, IEEE Transactions on Magnetics **35**, 3652 (1999).

[16] A. V. Ramos, J.-B. Moussy, M.-J. Guittet, M. Gautier-Soyer, C. Gatel, P. Bayle-Guillemaud, B. Warot-Fonrose, and E. Snoeck, Phys. Rev. B **75**, 224421 (2007).

[17] S. Xie, J. Cheng, B. W. Wessels, and V. P. Dravid, Appl. Phys. Lett. **93**, 181901 (2008).

[18] H. l. Guo, G. Liu, X. D. Li, H. M. Li, W. L. Zhang, J. G. Zhu, and D. Q. Xiao, Appl. Surf. Sci. **257**, 6573 (2011).

[19] S. Matzen, J.-B. Moussy, R. Mattana, F. Petroff, C. Gatel, B. Warot-Fonrose, J. C. Cezar, A. Barbier, M.-A. Arrio, and P. Sainctavit, Appl. Phys. Lett. **99**, 052514 (2011).

[20] Z. Yang, C. Ke, L. L. Sun, W. Zhu, H. B. Lu, and L. Wang, Thin Solid Films **519**, 2067 (2011).

[21] A.-K. Axelsson, F. Aguesse, V. Tileli, M. Valant, and N. M. Alford, J. Alloys Compd. **578**, 286 (2013).

[22] C. Gatel, B. Warot-Fonrose, S. Matzen, and J.-B. Moussy, Appl. Phys. Lett. **103**, 092405 (2013).

[23] M. G. Chapline and S. X. Wang, Phys. Rev. B **74**, 014418 (2006).

[24] H.-T. Jeng and G. Y. Guo, J. Magn. Magn. Mater. **239**, 88 (2002).

[25] D. Fritsch and C. Ederer, Phys. Rev. B **82**, 104117 (2010).

[26] D. Fritsch and C. Ederer, Appl. Phys. Lett. **99**, 081916 (2011).

[27] D. M. Wells, J. Cheng, D. E. Ellis, and B. W. Wessels, Phys. Rev. B **81**, 174422 (2010).

[28] P. V. Lukashev, J. D. Burton, A. Smogunov, J. P. Velev, and E. Y. Tsymbal, Phys. Rev. B **88**, 134430 (2013).

[29] A. Walsh, S.-H. Wei, Y. Yan, M. M. Al-Jassim, J. A. Turner, M. Woodhouse, and B. A. Parkinson, Phys. Rev. B **76**, 165119 (2007).

[30] Y. H. Hou, Y. J. Zhao, Z. W. Liu, H. Y. Yu, X. C. Zhong, W. Q. Qiu, D. C. Zeng, and L. S. Wen, J. Phys. D: Appl. Phys. **43**, 445003 (2010).

[31] N. M. Caffrey, D. Fritsch, T. Archer, S. Sanvito, and C. Ederer, Phys. Rev. B **87**, 024419 (2013).

[32] P. Blaha, K. Schwarz, G. K. H. Madsen, D. Kvasnicka, and J. Luitz, WIEN2K, *An Augmented Plane Wave + Local Orbitals Program for Calculating Crystal Properties* (Karlheinz Schwarz, Technische Universität Wien, Austria, 2001).

[33] J. P. Perdew, K. Burke, and M. Ernzerhof, Phys. Rev. Lett. **77**, 3865 (1996).

[34] V. I. Anisimov, I. V. Solovyev, M. A. Korotin, M. T. Czyżyk, and G. A. Sawatzky, Phys. Rev. B **48**, 16929 (1993).

[35] A. I. Liechtenstein, V. I. Anisimov, and J. Zaanen, Phys. Rev. B **52**, R5467 (1995).

[36] Q. Zeng, L. Zhang, X. Zhang, Q. Chen, Z. Feng, Y. Cai, L. Cheng, and Z. Weng, Phys. Lett. A **375**, 3521 (2011).

[37] D. Gutiérrez, M. Foerster, I. Fina, J. Fontcuberta, D. Fritsch, and C. Ederer, Phys. Rev. B **86**, 125309 (2012).

[38] N. C. Bristowe, E. Artacho, and P. B. Littlewood, Phys. Rev. B **80**, 045425 (2009).

[39] R. Arras, B. Warot-Fonrose, and L. Calmels, J. Phys.: Condens. Matter **25**, 256002 (2013).

[40] N. Nakagawa, H. Y. Hwang, and D. A. Muller, Nat. Mater. **5**, 204 (2006).

[41] P. R. Willmott, S. A. Pauli, R. Herger, C. M. Schlepütz, D. Martoccia, B. D. Patterson, B. Delley, R. Clarke, D. Kumah, C. Cionca, and Y. Yacoby, Phys. Rev. Lett. **99**, 155502 (2007).

[42] L. Qiao, T. C. Droubay, V. Shutthanandan, Z. Zhu, P. V. Sushko, and S. A. Chambers, J. Phys.: Condens. Matter **22**, 312201 (2010).

[43] J. A. Moyer, C. A. F. Vaz, E. Negusse, D. A. Arena, and V. E. Henrich, Phys. Rev. B **83**, 035121 (2011).

[44] A. V. Ramos, T. S. Santos, G. X. Miao, M.-J. Guittet, J.-B. Moussy, and J. S. Moodera, Phys. Rev. B **78**, 180402 (2008).

[45] E. J. W. Verwey and P. W. Haayman, Physica **8**, 979 (1941).

[46] A. Yanase and K. Siratori, J. Phys. Soc. Jpn. **53**, 312 (1984).

[47] M. I. Aroyo, A. Kirov, C. Capillas, J. M. Perez-Mato, and H. Wondratschek, Acta Cryst. **A62**, 115 (2006).

[48] V. G. Ivanov, M. V. Abrashev, M. N. Iliev, M. M. Gospodinov, J. Meen, and M. I. Aroyo, Phys. Rev. B **82**, 024104 (2010).

[49] M. N. Iliev, D. Mazumdar, J. X. Ma, A. Gupta, F. Rigato, and J. Fontcuberta, Phys. Rev. B **83**, 014108 (2011).

[50] L. Shen, M. Althammer, N. Pachauri, B. Loukya, R. Datta, M. Iliev, N. Bao, and A. Gupta, J. Cryst. Growth **390**, 61 (2014).

[51] Z. Szotek, W. M. Temmerman, D. Ködderitzsch, A. Svane, L. Petit, and H. Winter, Phys. Rev. B **74**, 174431 (2006).

[52] B. S. Holinsworth, D. Mazumdar, H. Sims, Q.-C. Sun, M. K. Yurtisigi, S. K. Sarker, A. Gupta, W. H. Butler, and J. L. Musfeldt, Appl. Phys. Lett. **103**, 082406 (2013).

[53] D. Odkhuu, P. Taivansaikhan, W. S. Yun, and S. C. Hong, J. Appl. Phys. **115**, 17A916 (2014).

[54] M. L. Boltz, R. H. French, D. J. Jones, R. V. Kasowski, and F. S. Phuchi, Phys. Scr. **41**, 4404 (1990).